Turbulence in the randomly forced, one-dimensional Burgers flow

Article *in* Journal of Statistical Physics · September 1975

DOI: 10.1007/BF01012841

CITATIONS
23

READS
18

2 authors:

Iwao Hosokawa
The University of Electro-Communications
137 PUBLICATIONS **1,014** CITATIONS
SEE PROFILE

Kiyoshi Yamamoto
61 PUBLICATIONS **759** CITATIONS
SEE PROFILE

Journal of Statistical Physics, Vol. 13, No. 3, 1975

Turbulence in the Randomly Forced, One-Dimensional Burgers Flow

I. Hosokawa[1] and K. Yamamoto[2]

Received April 2, 1974; revised April 1, 1975

The randomly forced, one-dimensional Burgers flow is dealt with by the method of the characteristic functional equation. The time development of the stochastic secondary flow is studied numerically by the Monte Carlo quadrature of the integral representation of solution for two types (white and "red") of random force fields. A turbulence-like behavior of the flow appears for a supercritical Reynolds number, and its structure is studied in detail.

KEY WORDS: Random force; Burgers flow; characteristic functional equation; Monte Carlo quadrature; turbulence; Fokker–Planck equation; random walk; nonlinear instability; ergodicity.

1. INTRODUCTION

Turbulent fluids excited by random forces have been studied by several authors.[1–4] The introduction of a random force field into a fluid is not only convenient for discussing a stationary (nondecaying) turbulence, but is also of practical significance in that stochastic disturbances (supposed to be found in the physical world) can be taken into account. In fact, the natural random force due to molecular fluctuation was formulated by Landau and Lifshitz.[5],3

[1] Department of Mechanical Engineering, Iwate University, Morioka, Japan.
[2] National Aerospace Laboratory, Tokyo, Japan.
[3] A more extensive result was given by Kelly and Lewis.[6]

In any case, the behavior of the fluid can then be described probabilistically by the generalized characteristic functional (gcf) equation[3,7] [see Eq. (1)] only if the quality of the random force is specified. Usually, the probability distribution of the random force is considered as Gaussian with zero mean, as is the case with Landau and Lifshitz's formulation, and in such cases the generalized characteristic functional equation takes a comparatively simple form.[3] With no random force, the equation reduces to the well-known Hopf equation.[8] The difference in mathematical character between the generalized characteristic functional equation with such a Gaussian random force and the Hopf equation is worth mentioning. That is, the Fourier transform of the former gcf is a typical Fokker–Planck or Kolmogorov equation (as is shown in Section 2), while that of the Hopf equation is only a first-order (functional) differential equation. This fact is important in showing that the generalized characteristic functional equation is irreversible, which ensures the approach to a unique, ultimate stationary state irrespective of initial states of the fluid even with zero viscosity. In other words, in the former case we deal with a simple Markovian stochastic process of fluid variables. Accordingly, it is proved that the flow is ergodic in the stationary state, where fluid variables can be considered as the so-called stationary random functions.[9] In the Hopf equation, however, the existence of such a unique stationary state is questionable. This is because the probability functional propagates along the characteristic curves in the (phase) function space, depending on initial conditions.[4] This fact alerts us to question the ergodicity of the process governed by the Hopf equation. At this point, it may be said that the generalized characteristic functional equation stands on a sounder basis than the Hopf equation because it is supported by the ergodic theorem.

In this paper, we study randomly forced, one-dimensional Burgers flow as an example of solving numerically the generalized characteristic functional equation. We are interested in the formation and structure of stationary inhomogeneous turbulence. Then, as Burgers first considered a model of channel flow,[11] the secondary flow is assumed to be limited in space, to interact with the *constant* main flow, and to vanish at the flow boundaries. This flow is stable in the sense of linear theory, resulting in vanishing secondary flow if the Reynolds number relevant to the main flow velocity and the space length is not high ($<\pi^2$). With a random force field present, however small, the situation is somewhat changed. The random force always excites the

[4] This fact is supported by a consideration of entropy. The entropy preservation of an ensemble of incompressible nonviscous flows was proved by Tatsumi and Ikeda.[10] If this is so, it is impossible for an ensemble of flows starting with an arbitrary entropy to approach irreversibly to a certain special ensemble with a definite entropy (such as the steady-state white-noise ensemble derived by Hopf[8]) without any other stochastic effect, e.g., stochastic boundary condition.

secondary flow to some degree, so that the perfect laminar state is never realized, but randomness of the flow velocity is insignificant if the Reynolds number is low. However, the flow may develop into another state for a supercritical Reynolds number ($>\pi^2$), since the secondary flow must be greatly excited in this case. We will consider two types of random force fields: white and "red." The ultimate stationary state depends on the type of random force field, but we may find a certain greater resemblance of both cases for high Reynolds numbers than we expect.

A challenging point in our study is the analytical difficulty in solving the basic functional equation. We avoid this difficulty by adopting a Monte Carlo method, utilizing the fact that the integral representation of the solution may be treated by means of sampling, i.e., a (generalized) random walk. Our random walk must be executed in a highly multidimensional space to obtain a good approximation. It is well known that the Monte Carlo quadrature is effective for such a many-dimensional case. The formulation is developed in Section 2 and the result is discussed in Section 3. In addition, a precise study of the nonlinear instability of the Burgers flow is presented in Section 4. There, it is verified that a number of Burgers' steady solutions[11] of the secondary flow equation are approached, each depending on particular (small-disturbance) initial conditions. It will be pointed out that because of the existence of more than one supercritical steady solution, the stationary turbulences obtained in this Burgers flow are of pseudo character.

2. FORMULATION

According to the previous work,[3] the so-called generalized characteristic functional equation is written as

$$\partial\psi/\partial t = i\int y(x)\chi[\delta/i\,\delta y(x)]\psi\,dx - \tfrac{1}{2}\iint y(x)y(x')F(x,x')\psi\,dx\,dx' \tag{1}$$

where $\psi[y(x), t]$ is the characteristic functional at time t of the stochastic velocity field $v(x)$ of the flow, x is the space coordinate, χ is an operator such that $\partial v/\partial t = \chi v$ is the dynamical equation governing $v(x, t)$ when no random force exists, $\delta/\delta y(x)$ is the functional differentiation with respect to y at x, and F is related to the correlation function of the random force field $f(x, t)$ as follows:

$$\langle f(x,t)f(x',t')\rangle = F(x,x')\,\delta(t-t') \tag{2}$$

with $\langle\ \rangle$ indicating the ensemble average. Here it is assumed that the probability distribution of f is Gaussian with zero mean. [More complicated cases of

the probability distribution of the random force lead to more generalized characteristic functional equations than Eq. (1).[3]] Naturally, F is positive definite.

In our Burgers flow,[11] x is a scalar variable, confined in $[0, b]$, and $v(x)$ is considered as the secondary flow velocity, since it only takes charge of stochasticity of the total flow. Then, χ is defined as

$$\chi v = \frac{U}{b} v + \nu \frac{\partial^2 v}{\partial x^2} - 2v \frac{\partial v}{\partial x} \tag{3}$$

where U is the main flow velocity and ν is the kinematic viscosity. We assume that U is constant, so that Burgers' equation for the main flow velocity may be replaced by the force equation

$$P = \nu \frac{U}{b} + \frac{1}{b} \int_0^b v^2 \, dx \tag{4}$$

which indicates the external force necessary to maintain the flow. As the secondary flow grows, P should increase. Obviously, our assumption makes the treatment of the Burgers flow very simple without losing its essence. (If U is a variable, we should have two simultaneous integrodifferential equations, even though P is assumed to be a constant.) The boundary conditions on v are

$$v = 0 \qquad \text{for} \quad x = 0 \text{ and } b \tag{5}$$

If the units are changed so that we measure velocity by U and distance by b, Eqs. (3)–(5) are rewritten as

$$\chi v = v + \frac{1}{R} \frac{\partial^2 v}{\partial x^2} - 2v \frac{\partial v}{\partial x} \tag{6}$$

$$P = (1/R) + \int_0^1 v^2 \, dx \tag{7}$$

$$v = 0 \qquad \text{for} \quad x = 0, 1 \tag{8}$$

where $R = Ub/\nu$, the Reynolds number of the flow.

If we expand $v(x)$ in terms of the basic wave modes which satisfy Eq. (8), $2^{1/2} \sin n\pi x$ for $n = 1, 2, \ldots$, the dynamical equation $\partial v/\partial t = \chi v$ may be replaced by

$$\frac{\partial v_n}{\partial t} = \chi_n v \equiv \left(1 - \frac{n^2\pi^2}{R}\right) v_n - \frac{n\pi}{2^{1/2}} \left(\sum_{m=1}^{n-1} v_m v_{n-m} - 2 \sum_{m=1}^{N} v_m v_{n+m} \right) \tag{9}$$

where v_n is the amplitude of each wave mode. N is infinite, but it may be replaced by a finite number in a truncation approach. Let us consider ψ as a

function of $\{y_n\}$ rather than a functional of $y(x)$ through the expansion $y(x) = \sum 2^{1/2} y_n \sin n\pi x$. Then Eq. (1) is rewritten as

$$\frac{\partial \psi}{\partial t} = i \sum_n y_n \chi_n \frac{\delta}{i \, \delta y(x)} \psi - \frac{1}{2} \sum_m \sum_n F_{mn} y_m y_n \psi \tag{10}$$

where

$$F_{mn} = 2 \int_0^1 \int_0^1 \sin(m\pi x) \sin(n\pi x') \, F(x, x') \, dx \, dx' \tag{11}$$

For convenience, let ψ be approximated by ψ_N, which is a function of $\{y_n; n \leqslant N\}$, and consider the Fourier transformation

$$\psi_N = \int \cdots \int p_N \exp\left(i \sum_{n=1}^{N} y_n v_n \right) \prod_{n=1}^{N} dv_n/(2\pi)^{1/2} \tag{12}$$

Then, we have the (probability) equation for p_N:

$$\frac{\partial p_N}{\partial t} = -\sum_n \frac{\partial}{\partial v_n} (\chi_n v p_N) + \frac{1}{2} \sum_n \sum_m \frac{\partial^2}{\partial v_m \, \partial v_n} (F_{mn} p_N) \tag{13}$$

which is a Fokker–Planck or Kolmogorov equation in many dimensions. When F_{mn} is diagonal, as is the case in this work, as $F_{mn} = \delta_{mn} B_n$ ($\geqslant 0$, because F is positive definite), the solution of this equation is simply given as the following successive integral with Gaussian measures[5]:

$$p_N(\{v_n\}, t) = \int_{\infty}^{\infty} \cdots \int \prod_{j=0}^{M-1} \prod_{n=1}^{N} \theta_n(v_n^{j+1}/v_n^j) p_N(\{v_n{}^0\}, 0) \, dv_n{}^j \tag{14}$$

in the limit $M \to \infty$, where

$$\theta_n(v_n^{j+1}/v_n^j) = (2\pi \, \Delta t \, B_n)^{-1/2} \exp[-(v_n^{j+1} - v_n^j - \Delta t \, \chi_n v^j)^2/(2 \, \Delta t \, B_n)] \tag{15}$$

where $\Delta t = t/M$ and $v_n{}^M = v_n$. If $B_n = 0$, θ_n reduces to a delta function: $\delta(v_n^{j+1} - v_n^j - \Delta t \, \chi_n v^j)$. In this work, the initial value of p_N is set as

$$p_N(\{v_n\}, 0) = \prod_{m=1}^{N} \delta(v_m{}^0) \tag{16}$$

assuming that initially the secondary flow is vanishing.

As is known from Eq. (12), any correlation of $v(x, t)$ or $\{v_n\}$ at time t can be given in terms of an integral with the measure (14). The integral is highly multidimensional and complicated looking, but it is executable with the aid of a Monte Carlo quadrature, even if only approximately. Since θ_n is Gaussian, to estimate the integral by importance sampling with the measure

[5] The propagation kernel method may be used for the derivation. See, e.g., Ref. 12.

$\prod\prod \theta_n\, dv_n^j$ involves making an ensemble of the random walks with the drift $\{\Delta t\, \chi_n v\}$ [starting from the origin in the (phase) space of $v(x)$] to average the estimator in the integral over the ensemble. As is seen from Eq. (15), each step of such a random walk is realized by the recurrence formula

$$v_n^{j+1} = v_n^j + \Delta t\, \chi_n v^j + (\Delta t\, B_n)^{1/2} r \tag{17}$$

where r is a standard normal random number. The approximation is expected to be improved by increasing M and N.

It is also to be noted that the random force term in Eq. (17) should be proportional to $\Delta t^{1/2}$. This is an essential property of the general Brownian motion. [If this term is excluded, it is evident that Eq. (17) gives Euler's method of solving Eq. (9).]

Finally, the energy balance of the secondary flow is easily formulated by integrating Eq. (13) after multiplying both sides by $\sum v_n^2/2$; that is,

$$(d/dt)\left(\tfrac{1}{2}\sum_n \langle v_n^2\rangle\right) = \sum_n \langle v_n \chi_n v\rangle + \tfrac{1}{2}\sum_n B_n \tag{18}$$

From Eq. (9), we have

$$\sum_n \langle v_n \chi_n v\rangle = \sum_n (1 - n^2\pi^2/R)\langle v_n^2\rangle \tag{19}$$

Then, it is clear that $B_n/2$ is the spectrum of the random-force power input to the flow. The positive effect of the right-hand side of Eq. (19) indicates the power input from the main flow.

3. RESULTS OF THE MONTE CARLO QUADRATURE

3.1. Selection of N and Δt

In the present calculation, $N = 20$ is used. In order to give an idea of how accurate the result to be obtained is, the laminar flow development for the case of $R = 100$ governed by Eq. (9) was calculated for both $N = 20$ and $N = 40$, putting, initially, $v_n = 0.01$, and using the finite-difference method (Euler's method) with $\Delta t = 0.004$. At $t = 20.0$, the calculated flow almost perfectly arrives at a steady state, the theoretical energy spectrum of which was given by Burgers as the solid line in Fig. 1 [Eq. (24) for $m = 1$]. Comparing both cases of approximation in the figure, we conclude that a substantial difference between the approximations and the exact values appears only for a few modes before the cutoff. (This discrepancy is considered to be due to accumulation of the energy to be transferred to higher wave-number modes.) Relying on this trial calculation, we will set $\Delta t = 0.004$ also in the Monte Carlo quadrature.

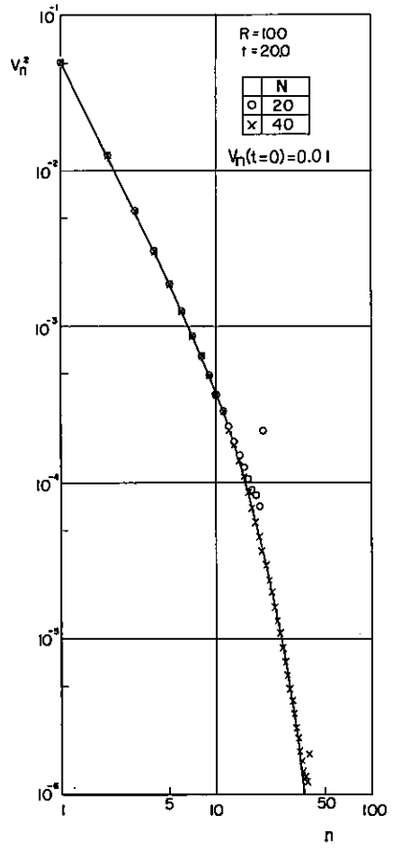

Fig. 1. Squared wave-number component of the secondary flow (without noise) velocity for $R = 100$ at $t = 20.0$ with the initial value $v_n^2 = 0.0001$ for all n, plotted against the wave number.

3.2. White Noise and "Red" Noise

We consider two types of random force fields; one is given by $B_n = 0.01$ for all $n \leqslant N$, and the other by $B_1 = B_2 = 0.01$ and $B_n = 0$ for $n \geqslant 3$. The former is called white noise and the latter "red" noise. By virtue of Eq. (11), $F(x, x')$ for these cases is expressed as

$$F(x, x') = 2\sum_{n=1}^{N} B_n \sin n\pi x \sin n\pi x' \tag{20}$$

When we are interested in the energy spectrum

$$E_n = \int_{-\infty}^{\infty}\cdots\int \tfrac{1}{2} v_n^2 p_N(\{v_n\}, t) \prod_{n=1}^{N} dv_n \tag{21}$$

then the estimator to be averaged over the ensemble is $\frac{1}{2}v_n^2$. The results are plotted in Figs. 2–5 for both types of noise for $R = 10$ and 100. The scale of

$\prod\prod \theta_n \, dv_n^j$ involves making an ensemble of the random walks with the drift $\{\Delta t \, \chi_n v\}$ [starting from the origin in the (phase) space of $v(x)$] to average the estimator in the integral over the ensemble. As is seen from Eq. (15), each step of such a random walk is realized by the recurrence formula

$$v_n^{j+1} = v_n^j + \Delta t \, \chi_n v^j + (\Delta t \, B_n)^{1/2} r \tag{17}$$

where r is a standard normal random number. The approximation is expected to be improved by increasing M and N.

It is also to be noted that the random force term in Eq. (17) should be proportional to $\Delta t^{1/2}$. This is an essential property of the general Brownian motion. [If this term is excluded, it is evident that Eq. (17) gives Euler's method of solving Eq. (9).]

Finally, the energy balance of the secondary flow is easily formulated by integrating Eq. (13) after multiplying both sides by $\sum v_n^2/2$; that is,

$$(d/dt)\left(\tfrac{1}{2}\sum_n \langle v_n^2 \rangle\right) = \sum_n \langle v_n \chi_n v \rangle + \tfrac{1}{2}\sum_n B_n \tag{18}$$

From Eq. (9), we have

$$\sum_n \langle v_n \chi_n v \rangle = \sum_n (1 - n^2\pi^2/R)\langle v_n^2 \rangle \tag{19}$$

Then, it is clear that $B_n/2$ is the spectrum of the random-force power input to the flow. The positive effect of the right-hand side of Eq. (19) indicates the power input from the main flow.

3. RESULTS OF THE MONTE CARLO QUADRATURE

3.1. Selection of N and Δt

In the present calculation, $N = 20$ is used. In order to give an idea of how accurate the result to be obtained is, the laminar flow development for the case of $R = 100$ governed by Eq. (9) was calculated for both $N = 20$ and $N = 40$, putting, initially, $v_n = 0.01$, and using the finite-difference method (Euler's method) with $\Delta t = 0.004$. At $t = 20.0$, the calculated flow almost perfectly arrives at a steady state, the theoretical energy spectrum of which was given by Burgers as the solid line in Fig. 1 [Eq. (24) for $m = 1$]. Comparing both cases of approximation in the figure, we conclude that a substantial difference between the approximations and the exact values appears only for a few modes before the cutoff. (This discrepancy is considered to be due to accumulation of the energy to be transferred to higher wave-number modes.) Relying on this trial calculation, we will set $\Delta t = 0.004$ also in the Monte Carlo quadrature.

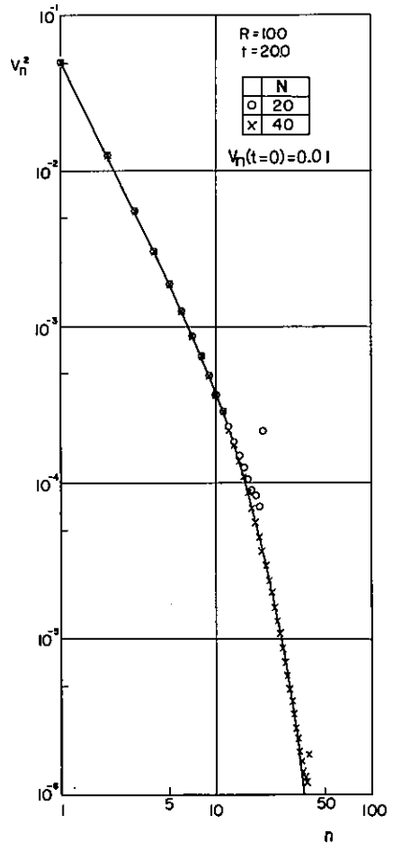

Fig. 1. Squared wave-number component of the secondary flow (without noise) velocity for $R = 100$ at $t = 20.0$ with the initial value $v_n^2 = 0.0001$ for all n, plotted against the wave number.

3.2. White Noise and "Red" Noise

We consider two types of random force fields; one is given by $B_n = 0.01$ for all $n \leqslant N$, and the other by $B_1 = B_2 = 0.01$ and $B_n = 0$ for $n \geqslant 3$. The former is called white noise and the latter "red" noise. By virtue of Eq. (11), $F(x, x')$ for these cases is expressed as

$$F(x, x') = 2\sum_{n=1}^{N} B_n \sin n\pi x \sin n\pi x' \tag{20}$$

When we are interested in the energy spectrum

$$E_n = \int_{-\infty}^{\infty} \cdots \int \tfrac{1}{2} v_n^2 p_N(\{v_n\}, t) \prod_{n=1}^{N} dv_n \tag{21}$$

then the estimator to be averaged over the ensemble is $\frac{1}{2}v_n^2$. The results are plotted in Figs. 2–5 for both types of noise for $R = 10$ and 100. The scale of

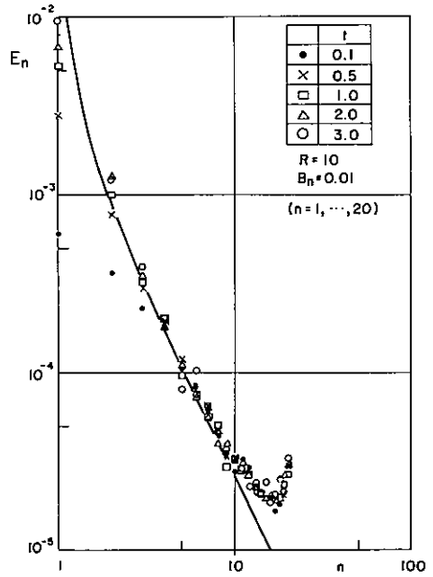

Fig. 2. Energy spectrum of the stochastic secondary flow with white noise for $R = 10$.

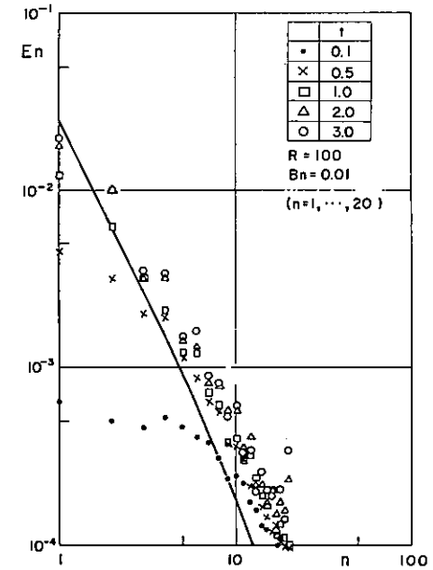

Fig. 3. Energy spectrum of the stochastic secondary flow with white noise for $R = 100$.

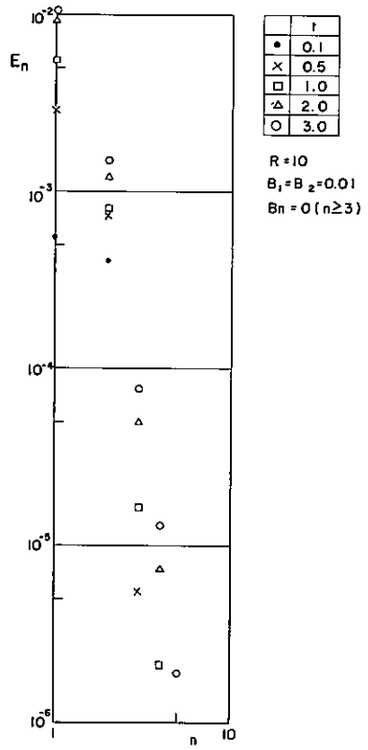

Fig. 4. Energy spectrum of the stochastic secondary flow with "red" noise for $R = 10$.

the ensemble, that is, the number of all random walks executed, is 200; in fact, this scale is large enough to guarantee a good approximation to the ensemble average. Although the critical Reynolds number is π^2 in linear theory, $R = 10$ ($\gtrsim \pi^2$) seems to be still on the stable side, as is seen from a comparison of these figures. In fact, the excited energy for $R = 10$ is much lower than that for $R = 100$ for both types of noise. The energy spectrum with "red" noise shows too weak a nonlinear interaction working to convey energy to higher wave-number modes, even at the stationary state of $t = 3.0$. We note that in Fig. 2 the n^{-2} spectrum for $R = 10$ for white noise is not formed by the nonlinear interaction in the Burgers equation but arises for the following reason: For R small, when the nonlinear interaction is relatively negligible, any interaction between different waves vanishes from Eq. (18). Then, at the stationary state, we may have the separate relation for each mode

$$\langle v_n^2 \rangle = \tfrac{1}{2} B_n / (1 - n^2 \pi^2 / R) \tag{22}$$

which is indicated by the solid line in Fig. 2. Equation (22) gives the n^{-2} spectrum except for $n^2 \approx R/\pi^2$, where the plotted points at $t = 3.0$ nearly

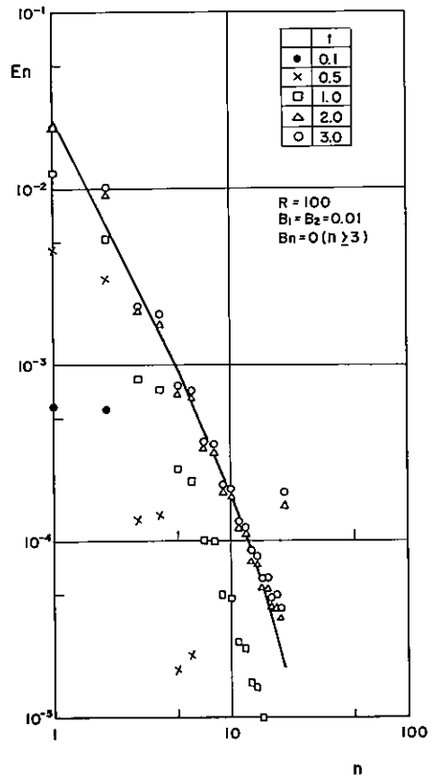

Fig. 5. Energy spectrum of the stochastic secondary flow with "red" noise for $R = 100$.

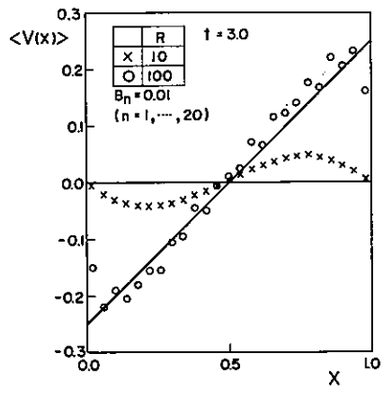

Fig. 6. Average velocity profile of the stochastic secondary flow with white noise.

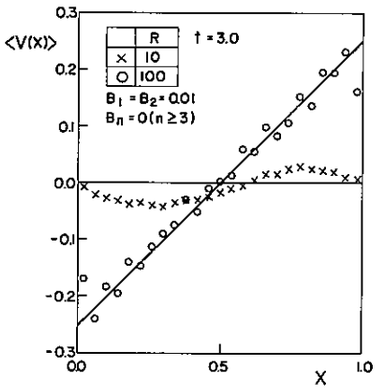

Fig. 7. Average velocity profile of the stochastic secondary flow with "red" noise.

coincide with the solid line; the discrepancy from the n^{-2} law in the high-wave-number region is obviously the error of our approximation ($N = 20$). For $R = 100$, the energy spectra for both types of noise rather resemble each other in shape, and they may be characterized by the n^{-2} law until $n = 10$. For convenience of comparison, a common solid line was inserted in Figs. 3 and 5, which is the theoretical curve given from Eq. (24) or (26) (for $m = 1$).

If another estimator is considered as $v(x)$, the average velocity field of the secondary flow is calculated by the same ensemble of random walks, as is plotted in Figs. 6 and 7. For $R = 10$ at $t = 3.0$, we have somewhat excited states caused by the random force action in place of the perfect laminar state, $v(x) = 0$; and there, the higher wave-number modes are too weak to affect the average velocity profile. The profiles for $R = 100$ at $t = 3.0$ are similar in both figures, resulting in the steady positive-gradient straight line shown, which is the theoretical curve given from Eq. (29) (for $m = 1$), except near the boundaries of the flow where shock dissipation occurs. The reason for this will be clarified in Section 5.

3.3. Development of Turbulence

The sum of E_n can be plotted against t to show the time development of the secondary flow energy, as is seen in Figs. 8 and 9. The solid lines indicate the total random-force energy input to the flow until time t. (Note that the power of white noise is ten times as much as that of "red" noise.) Hence, we know that the energy level of the fully developed secondary flow is almost indifferent to the type and intensity of random force. This fact holds both for nearly laminar flow ($R = 10$) and for turbulent flow ($R = 100$). To confirm this, Fig. 10 shows the result for $R = 100$ with white noise of a much lower

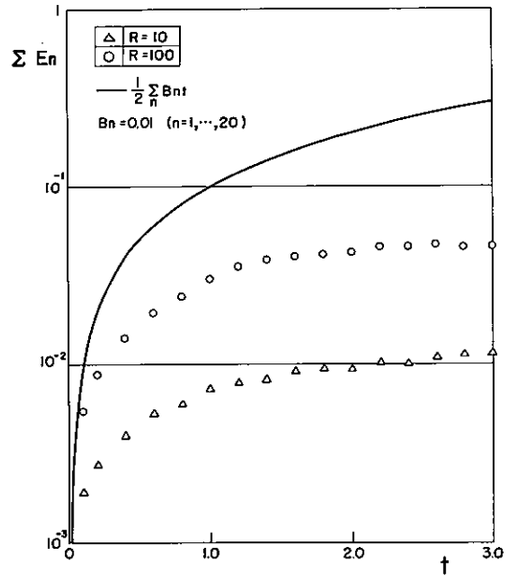

Fig. 8. Time development of the energy of the stochastic secondary flow with white noise.

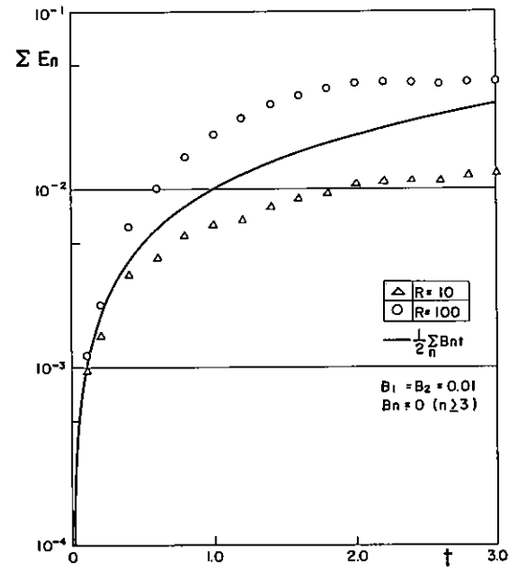

Fig. 9. Time development of the energy of the stochastic secondary flow with "red" noise.

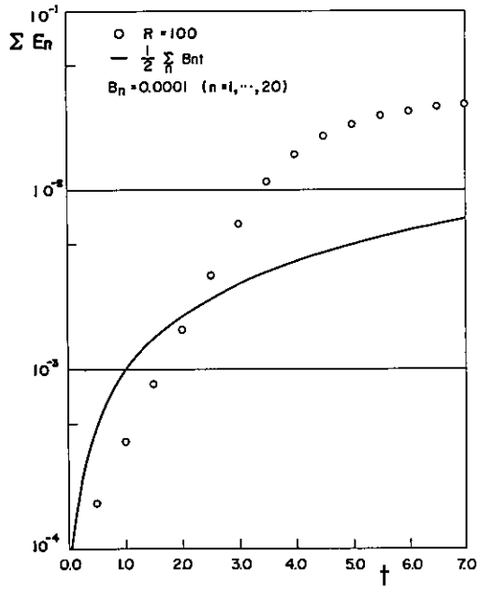

Fig. 10. Time development of the energy of the stochastic secondary flow with very weak white noise.

power level. In this case, the turbulence energy grows far beyond the total random-force energy input to the flow, until it reaches almost the same level as reached in the other cases at $t = 7.0$. For reference, the energy spectrum of this case is shown in Fig. 11.

It is instructive to compare Figs. 3, 5, and 11. We have said that the energies of these fully developed turbulences are almost on the same level, but strictly speaking, there is still a distinction. We can enlarge this distinction by looking into the variance of the velocity field.

3.4. Variance

The variance field $\langle [v(x) - \langle v(x) \rangle]^2 \rangle$ is shown for each case in Figs. 12–14. While that of nearly laminar flow ($R = 10$) is almost independent of the type of random force, that of turbulent flow ($R = 100$) varies. The difference of the variance level for each case depends almost linearly on the small distinctions in turbulent energy level seen in Figs. 3, 5, and 11; this is because $\langle v(x)^2 \rangle = 2 \sum E_n$, while $\langle v(x) \rangle$ is almost the same for all cases (see Figs. 6 and 7). The origin of the distinction will be clarified in Section 5.

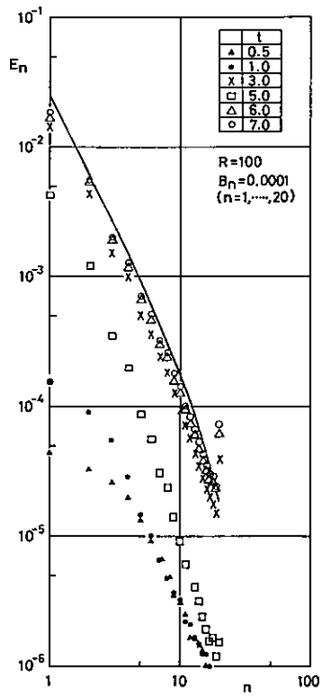

Fig. 11. Energy spectrum of the stochastic secondary flow with very weak white noise for $R = 100$.

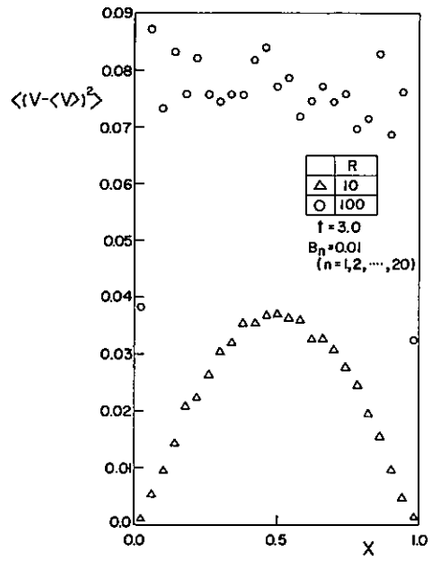

Fig. 12. Velocity variance field of the stochastic secondary flow with white noise.

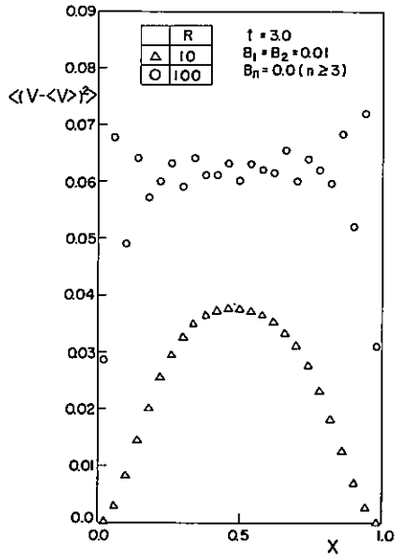

Fig. 13. Velocity variance field of the stochastic secondary flow with "red" noise.

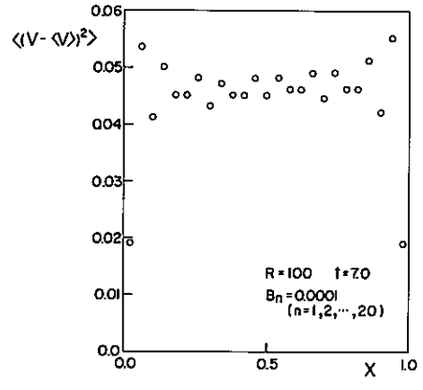

Fig. 14. Velocity variance field of the stochastic secondary flow with very weak white noise.

4. NONLINEAR INSTABILITY

The overall character of the ensemble dynamics of the randomly forced, one-dimensional Burgers flow has been clarified to a large degree, but in order to understand further the formation of turbulence, it is useful to know the development of nonlinear instability of individual flows without random forces, starting from the quiescent state with a small disturbance. We inquired into the growth of $\{v_n\}$, according to Eq. (9) (with $N = 20$), with various initial conditions for various R. Some results are seen in Figs. 15–24 [$v_n(t)$ for n high was omitted, because the values are near zero]. First, it is natural that all velocity modes are attenuated in subcritical flows and return to the stable laminar state. (See Figs. 15 and 16. For $R = 1$, the time step Δt was taken as 0.0005 to avoid numerical instability.) For $R = 10$ (which case

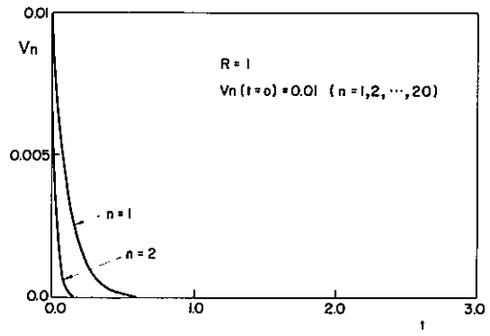

Fig. 15. Time development of each mode of the secondary flow (without noise) velocity with the initial value $v_n = 0.01$ for all n for $R = 1$.

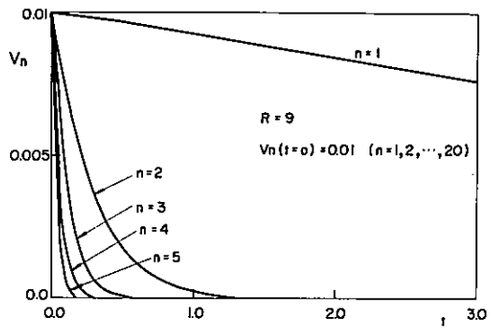

Fig. 16. Time development of each mode of the secondary flow (without noise) velocity with the initial value $v_n = 0.01$ for all n for $R = 9$.

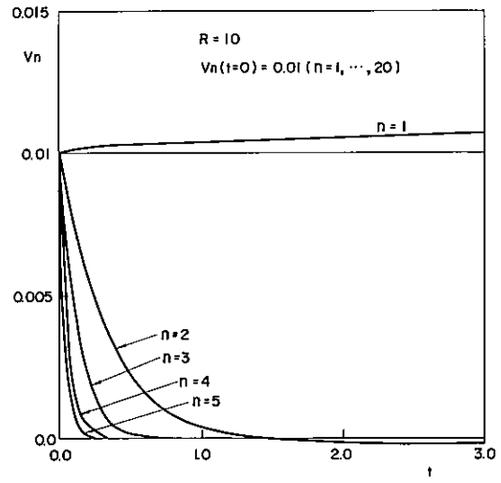

Fig. 17. Time development of each mode of the secondary flow (without noise) velocity with the initial value $v_n = 0.01$ for all n for $R = 10$.

we call "nearly subcritical" in Section 3), only the first mode grows very slightly (see Fig. 17).

However, the development of each mode for $R = 100$ is quite dramatic. (See Figs. 18–24.) The linear growth of instability in the flow is prevented by the nonlinear effect of Eq. (9); all modes converge to various steady values. A comparison of Figs. 18 and 19 shows how the time for the flow to reach a steady state depends on initial conditions. Figures 20–22 show that there are at least three steady states other than the one in Figs. 18 and 19; their realization depends on initial conditions. According to Burgers,[11] there are many other steady solutions depending on R.

All those theoretically given for large R may be expressed in terms of the following four families:

$$\text{(I)} \qquad v^{Im}(x) = \frac{1}{2}\left\{x - \frac{1}{2m-1}\sum_{k=1}^{m}\left[1 + \tanh\frac{R}{2(2m-1)}\left(x - \frac{2k-1}{2m-1}\right)\right]\right\} \tag{23}$$

or

$$v_n^{Im} = -\frac{\pi}{2^{1/2}R}\frac{1}{\sinh[(2m-1)n\pi^2/R]} \times\left[(-1)^n + 2\sum_{k=1}^{m-1}\cos\left(\frac{2k-1}{2m-1}n\pi\right)\right] \tag{24}$$

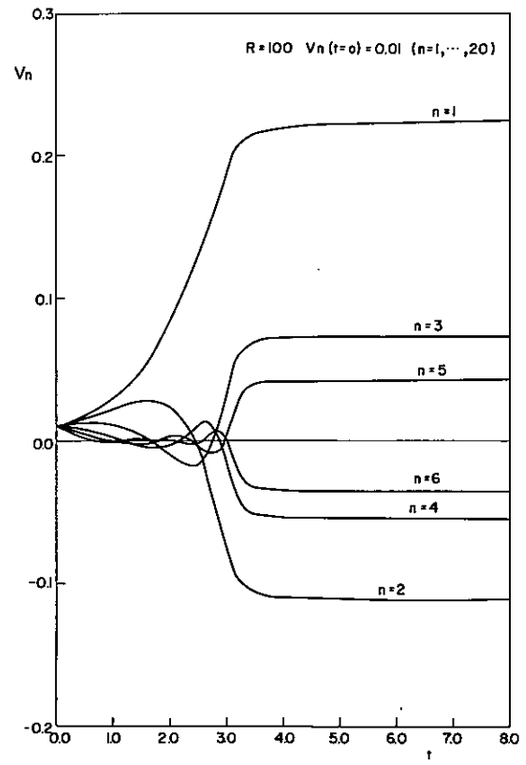

Fig. 18. Time development of each mode of the secondary flow (without noise) velocity with the initial value $v_n = 0.01$ for all n for $R = 100$.

$$\text{(II)} \qquad v^{\mathrm{II}m}(x) = \frac{1}{2}\left\{x + \frac{1}{2m-1} - \frac{1}{2m-1}\sum_{k=1}^{m}\left[1 + \tanh\frac{R}{2(2m-1)} \times \left(x + \frac{1}{2m-1} - \frac{2k-1}{2m-1}\right)\right]\right\} \tag{25}$$

or

$$v_n^{\mathrm{II}m} = -\frac{\pi}{2^{1/2}R}\frac{1}{\sinh[(2m-1)n\pi^2/R]} \times \left\{1 + 2\sum_{k=2}^{m}\cos\left[\left(\frac{2k-1}{2m-1} - \frac{1}{2m-1}\right)n\pi\right]\right\} \tag{26}$$

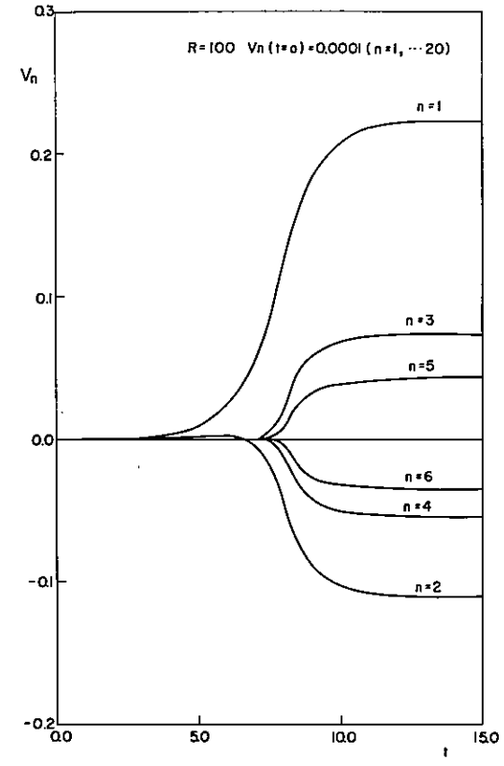

Fig. 19. Time development of each mode of the secondary flow (without noise) velocity with the initial value $v_n = 0.0001$ for all n for $R = 100$.

$$\text{(III)} \qquad v^{\mathrm{III}m}(x) = \frac{1}{2}\left\{x - \frac{1}{2m}\sum_{k=1}^{m}\left[1 + \tanh\frac{R}{4m}\left(x - \frac{2k-1}{2m}\right)\right]\right\} \tag{27}$$

or

$$v_n^{\mathrm{III}m} = -\frac{2^{1/2}\pi}{R}\frac{1}{\sinh(2mn\pi^2/R)}\sum_{k=1}^{m}\cos\left(\frac{2k-1}{2m}n\pi\right) \tag{28}$$

$$\text{(IV)} \qquad v^{\mathrm{IV}m}(x) = \frac{1}{2}\left\{x + \frac{1}{2m} - \frac{1}{2m}\sum_{k=1}^{m+1}\left[1 + \tanh\frac{R}{4m} \times \left(x - \frac{2k-1}{2m} + \frac{1}{2m}\right)\right]\right\} \tag{29}$$

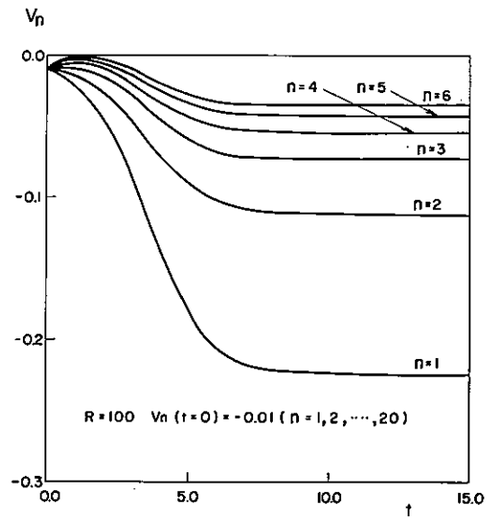

Fig. 20. Time development of each mode of the secondary flow (without noise) velocity with the initial value $v_n = -0.01$ for all n for $R = 100$.

or

$$v_n^{\mathrm{IV}m} = -\frac{\pi}{2^{1/2}R}\frac{1}{\sinh(2mn\pi^2/R)}$$

$$\times\left\{1 + (-1)^n + 2\sum_{k=2}^{m}\cos\left[\left(\frac{2k-1}{2m} - \frac{1}{2m}\right)n\pi\right]\right\} \qquad (30)$$

the profiles of which are sketched in Fig. 25. The reason why equal shocks are displayed in [0, 1] in such a rational way, as sketched, is explained in Murray's[13] recent treatment of the same Burgers flow by the phase plane method. The summation terms in Eqs. (24), (26), and (30) are understood to vanish for $m = 1$. As may also be understood from Fig. 25, m is the number of shocks in [0, 1] for families I, II, and III; family IV has $m + 1$. As is easily seen, the nonvanishing modes of $v_n^{\mathrm{I}1}$ and $v_n^{\mathrm{II}1}$ begin with $n = 1$, but those of $v_n^{\mathrm{III}1}$ and $v_n^{\mathrm{IV}1}$ begin with $n = 2$. Further, those of $v_n^{\mathrm{I}2}$ and $v_n^{\mathrm{II}2}$ begin with $n = 3$, but those of $v_n^{\mathrm{III}2}$ and $v_n^{\mathrm{IV}2}$ begin with $n = 4$;.... On the other hand, when $R = 100$, we have

$$1 - n^2\pi^2/R < 0 \qquad \text{for} \quad n \geqslant 4 \qquad (31)$$

Hence, it is known that solutions $v_n^{\mathrm{III}2}$ and $v_n^{\mathrm{IV}2}$, and the others beginning with

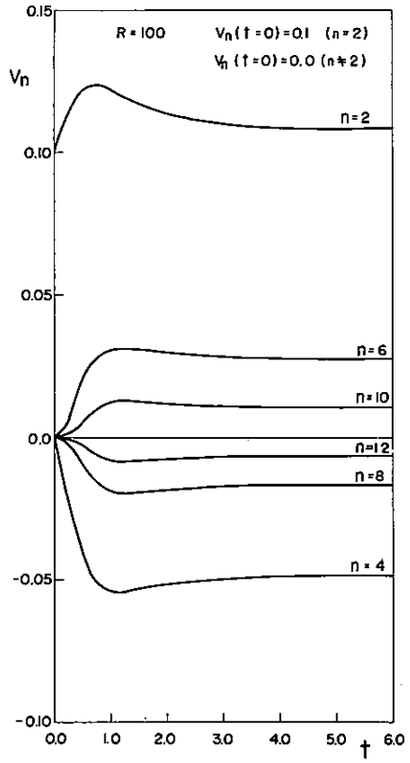

Fig. 21. Time development of each mode of the secondary flow (without noise) velocity with the initial value $v_n = 0.1$ for $n = 2$, and with $v_n = 0.0$ for $n \neq 2$, for $R = 100$.

$n = 4, 5,...$, never satisfy the steady condition of Eqs. (18)–(19). Then, possible steady solutions for $R = 100$ are restricted to $v^{\mathrm{I}1}$, $v^{\mathrm{III}1}$, $v^{\mathrm{IIII}1}$, $v^{\mathrm{IV}1}$, $v^{\mathrm{I}2}$, and $v^{\mathrm{II}2}$. Figures 18 and 19 correspond to $v^{\mathrm{I}1}$, Fig. 20 to $v^{\mathrm{III}1}$, Fig. 21 to $v^{\mathrm{IIII}1}$, and Fig. 22 to $v^{\mathrm{IV}1}$.

The existence of such a number of steady solutions is characteristic of the present one-dimensional Burgers flow. Usually, we would never expect more than one steady solution to exist for a supercritical flow. We numerically investigated the stability of the solutions; $v^{\mathrm{I}1}$ and $v^{\mathrm{III}1}$ are stable and $v^{\mathrm{IIII}1}$ is certainly unstable, as is seen in Fig. 24, in which the disturbed flow develops into $v^{\mathrm{I}1}$. When another disturbed flow is taken as $v_n(t = 0) = -0.001$ for n odd, it develops into $v^{\mathrm{III}1}$. $v^{\mathrm{IV}1}$ looks almost stable, as is seen in Fig. 23, but the modes with n odd are not attenuated, at least until $t = 15.0$; we call this quasistable. $v^{\mathrm{I}2}$ and $v^{\mathrm{II}2}$ are unstable, and finally they transform into $v^{\mathrm{I}1}$ or $v^{\mathrm{III}1}$, depending on the initial disturbance. Lee[14] and Murray[13] considered only $v^{\mathrm{I}1}$ as the unique stable steady solution. However, our computation

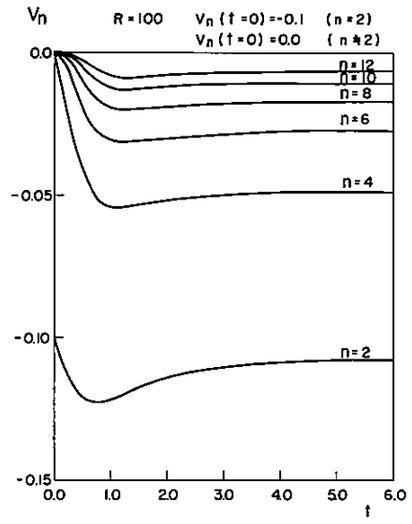

Fig. 22. Time development of each mode of the secondary flow (without noise) velocity with the initial value $v_n = -0.1$ for $n = 2$, and with $v_n = 0.0$ for $n \neq 2$, for $R = 100$.

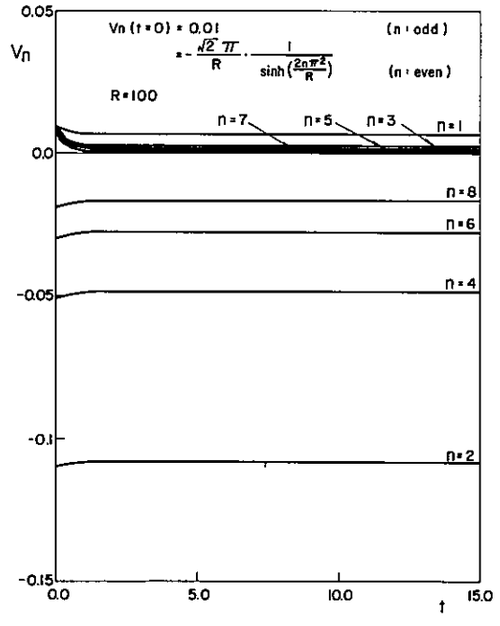

Fig. 23. Instability test for each mode of solution v^{IV1}.

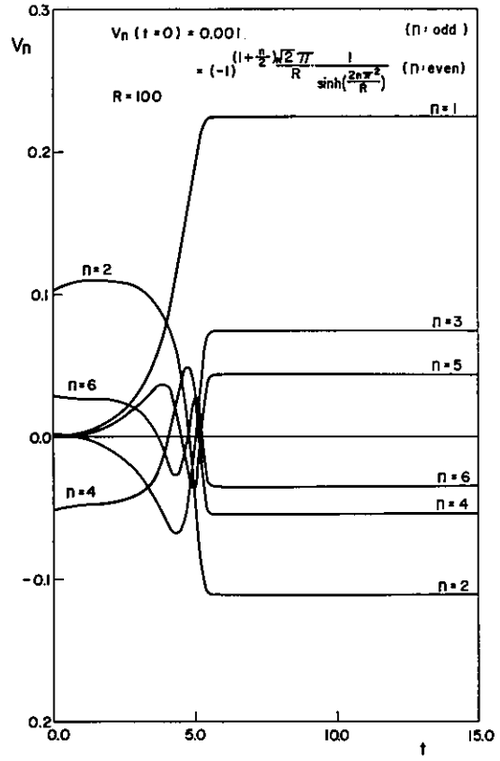

Fig. 24. Instability test for each mode of solution v^{III1}.

never showed any uniqueness in the final state of $v(x)$. v^{III} is also stable and approachable in the same right as v^{II}. This fact was confirmed for the case $N = 40$. This may be understood by noticing that v^{II} and v^{III} are dual solutions of the basic Burgers equation defined by Eq. (6) [$v^{III}(x) = -v^{II}(1 - x)$].[6]

Thus, we may expect that these two stable and one quasistable steady solutions mix together in the ensemble of the randomly forced secondary flows at the final stationary state for $R = 100$, even though these solutions are always deformed to some degree by the random force action. To verify this fact, it is useful to see directly the structure of the ensembles obtained, by means of histograms, as is shown in the next section.

[6] Murray acknowledged in a private communication that both solutions, v^{II} and v^{III}, are equally realizable and that the word "unique" was not proper.

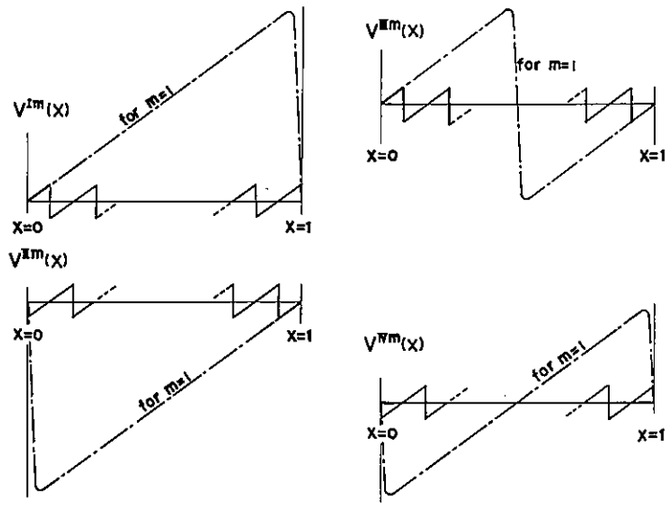

Fig. 25. Illustrations of the steady solutions of the Burgers equation ($\partial v/\partial t = \chi v$).

5. PSEUDO TURBULENCE

The histograms of v_n for $n = 1, 2$, and 3 in the stationary ensembles (corresponding to Figs. 3, 5, and 11) are shown in Figs. 26–28. The theoretical values for v_n of our stable and quasistable steady solutions (i.e., $v_n^{\mathrm{I}1}$, $v_n^{\mathrm{III}1}$, and $v_n^{\mathrm{IV}1}$) are indicated by dashed lines in the figures for comparison. Hence, it is known that if the level of the random force is very low [as in case (c) in the figures], the expectation (in Section 4) is fairly sharply realized. In this case, the ratio of the population of the neighbors to solutions $v_n^{\mathrm{I}1}$ and $v_n^{\mathrm{III}1}$ to that of $v_n^{\mathrm{IV}1}$ is very large. Therefore, it is evident that the energy spectrum resulting from this ensemble is very close to that of the simple flow of solution $v_n^{\mathrm{I}1}$ or $v_n^{\mathrm{III}1}$, as indicated by the solid line in Fig. 11. The sharpness of the v_n distribution also explains the comparative smallness of the velocity variance shown in Fig. 14. On the other hand, in the case of the higher noise level, i.e., cases (a) and (b), the population of v_n diffuses more widely around solutions $v_n^{\mathrm{I}1}$, $v_n^{\mathrm{III}1}$, and $v_n^{\mathrm{IV}1}$. The fact that the population of the neighbors to $v_n^{\mathrm{IV}1}$ is relatively large results in the sawtooth-like configuration of the circles in Figs. 3 and 5, because $v_n^{\mathrm{IV}1}$ has no components with n odd, according to Eq. (30), to contribute to E_n with n odd. The tendency of the energy spectra of these ensembles to exceed the solid line is explained by the tendency to diffuse toward regions of v_n more energetic than $v_n^{\mathrm{I}1}$ and $v_n^{\mathrm{III}1}$. The comparative largeness of the velocity variance in Figs. 12 and 13 is also so explained. Since we have seen that all the ensembles for $R = 100$ are constituted by solutions $v^{\mathrm{I}1}$, $v^{\mathrm{III}1}$, and

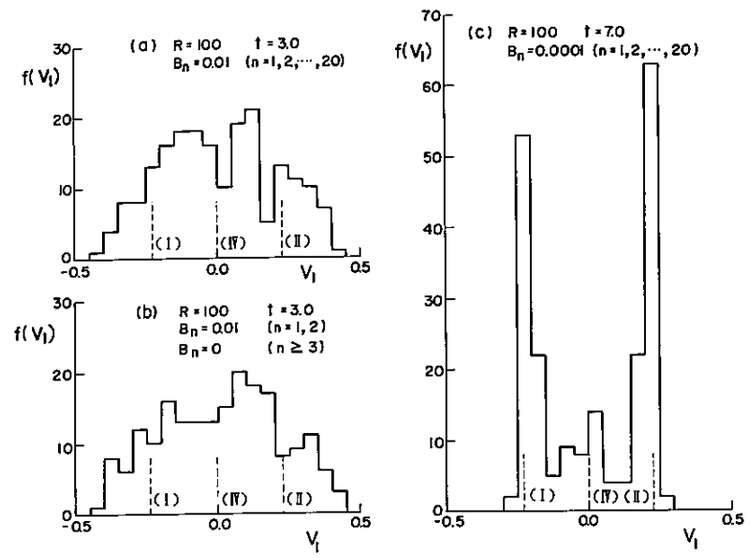

Fig. 26. Histograms of the first mode of the stochastic secondary flow velocity in the ensembles.

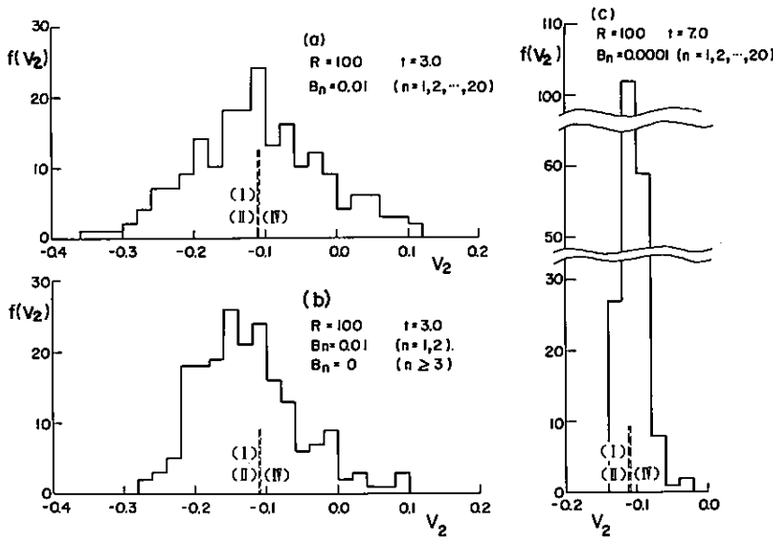

Fig. 27. Histograms of the second mode of the stochastic secondary flow velocity in the ensembles.

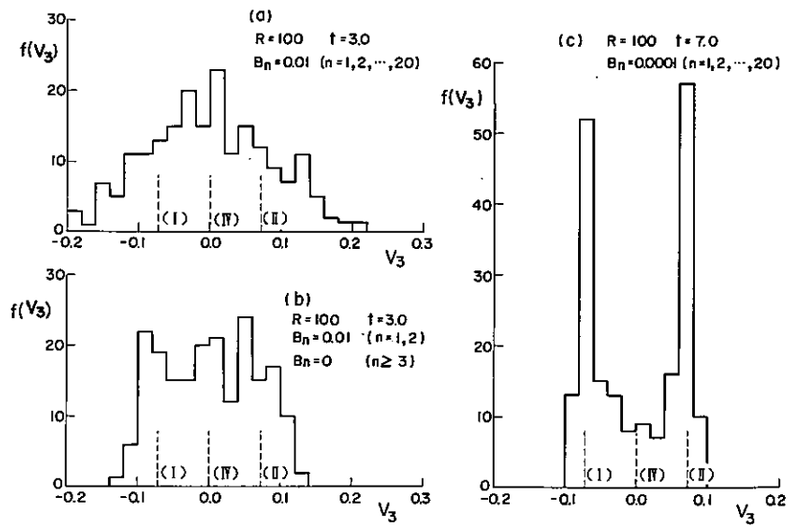

Fig. 28. Histograms of the third mode of the stochastic secondary flow velocity in the ensembles.

v^{IV1} and their neighbors, and that the neighbors to v^{I1} are nearly as equally populated as are those to v^{III1}, then it is easy to understand that the average velocity profile for the ensemble, as plotted in Figs. 6 and 7, tends to result in the simple velocity profile of solution v^{IV1}. Note that the average of v^{I1} and v^{III1} is just v^{IV1} except in the shock-dissipation regions.

A remarkable fact observed from the histograms is that the distributions of v_n and then $v(x)$ in the stationary ensembles for $R = 100$ are far from normal, but are concentrated in solutions v^{I1}, v^{III1}, and v^{IV1}, resulting in two or three peaks. This is obviously rooted in the special nature of the one-dimensional Burgers flow which has more than one stable steady supercritical solution.

Burgers identified each of the steady solutions as a turbulence solution, but such a turbulence is not the type that we imagine in real flows. A real turbulence is never steady, but behaves so irregularly and so unsteadily that it is necessary to follow the average flow behavior over a long time. For this reason, the statistical theory of turbulence began with hypothesizing the ergodicity, i.e., that such a time average can be equated to the ensemble average. We know that the statistical theory can be exactly formulated in the characteristic functional equation, with or without random force. The time we use in the characteristic functional equation is considered to be of such a large scale as to be able to describe the long-time behavior. For the stationary

state, the ergodic hypothesis is proved to be true by the method of stationary random functions,[9] if it is the case with the generalized characteristic functional equation which describes a Markovian stochastic process. In fact, according to Panchev,[9] the stationary random functions which guarantee the ergodic theorem should have the following two conditions: (1) the single probability density of functions is unique and time independent, and (2) the double probability density of functions only depends on the time difference. The single and double probability densities to be derived from our generalized characteristic functional equation usually satisfy the two conditions. (As for the uniqueness proof of steady-state solution in the cylinder functional approach as assumed in Eqs. (12)–(13), the reader is referred to Ref. 15.) However, for the case of the Hopf equation, there remains some question, in general, of the uniqueness of the steady-state solution for the reason described in the introduction. [Then, from our standpoint, it may be considered that such stationary random functions found in practice, such as wind velocity, etc.,[9] are not actually exactly governed by the Hopf equation (based on a deterministic dynamics) but rather the generalized characteristic functional equation (based on Langevin-type dynamics).]

Therefore, in stationary, randomly forced Burgers flow, we must consider that, even though an individual flow has approached very near one of v^{I1}, v^{III1}, and v^{IV1}, it will move out of there, by virtue of an accumulated random-force effect, in order for the time average to be equal to the ensemble average. Without random force action, however, this never happens. In fact, as was shown in the last section, individual flows approach either solution v^{I1} or v^{III1} asymptotically (v^{IV1} would eventually be unstable). Then the long-time average of an arbitrary individual flow is two-valued, while the ensemble average should be single-valued, as v^{IV1}. Hence, it is obvious that the Hopf equation, at least dealing with the present one-dimensional Burgers flow, produces neither ergodicity nor stationary random functions.

To be sure, our stationary, randomly forced Burgers flow is ergodic, but the time of averaging should be very large if the random force is weak. If the time of averaging is not large enough, the time-averaged behavior of an individual flow will present the flow given by v^{I1}, v^{III1}, or some intermediate between them. This is a disturbing situation, which confuses an observer of experiment. Such an unstable condition would hardly happen if there is at most one or no stable supercritical steady solution of the basic dynamical equation in question (as is usually expected in real flow). Therefore, it may be more suitable to call the excited state of the present randomly forced Burgers flow a pseudo turbulence. The pseudo turbulence is characterized by the fact that the distribution of v is far from normal because there are several peaks. In this case, of course, any quasinormality approach,[16] as well as the Wiener–Hermite expansion method,[17] will not be effective. However, it is

worth noting that the statistical theory of turbulence, based on ensemble mechanics, *sometimes* brings forth a pseudo turbulence.

6. CONCLUSION

In this work, we showed that the generalized characteristic functional equation (1) is numerically solvable with the aid of the Monte Carlo quadrature. As a result, the important, but peculiar, feature of the randomly forced, one-dimensional inhomogeneous Burgers flow was clarified. For the two-dimensional Burgers flow, however, we may have a more realistic turbulence, since there is Burgers' proof that this flow has no nonvanishing steady solution.[11] We plan to treat a randomly forced Navier–Stokes flow by the same method, although it is apparent that the success will depend not only on the capacity of the computer available, but also on the development of some new technique of approximating a highly multidimensional integral.

REFERENCES

1. E. A. Novikov, *Soviet Phys.—JETP* **20**:1290 (1965).
2. S. F. Edwards, *J. Fluid Mech.* **18**:239 (1964).
3. I. Hosokawa, *J. Phys. Soc. Japan* **25**:271 (1968).
4. D. T. Jeng, *Phys. Fluids* **12**:2006 (1969).
5. L. D. Landau and E. M. Lifshitz, *Fluid Mechanics*, Pergamon, New York (1959), Chapter 17.
6. G. E. Kelly and M. B. Lewis, *Phys. Fluids* **14**:1925 (1971).
7. I. Hosokawa, *Nagare* (*J. Fluid Mechanics Assoc., Japan*) 3(2):40 (1971).
8. E. Hopf, *J. Rat. Mech. Anal.* **1**:87 (1952).
9. S. Panchev, *Random Functions and Turbulence*, Pergamon Press, Oxford (1971), p. 41.
10. T. Tatsumi and N. Ikeda, Inst. Space Aero. Sci., Univ. Tokyo, Rep. **2**:A-73 (1966).
11. J. M. Burgers, *Advanced Applied Mechanics*, Vol. 1, Academic Press (1948), p. 171.
12. I. Hosokawa, *J. Math. Phys.* **11**:657 (1970).
13. J. D. Murray, *J. Fluid Mech.* **59**:263 (1973).
14. J. Lee, *J. Fluid Mech.* **47**:321 (1971).
15. A. H. Gray, Jr., *J. Math. Phys.* **6**:644 (1965).
16. I. Proudman and W. H. Reid, *Phil. Trans. Roy. Soc. A* **247**:163 (1954); T. Tatsumi, *Proc. Roy. Soc. A* **239**:16 (1957); M. Millionshchikov, *Doklady Acad. Sci. SSSR* **32**:619 (1941).
17. W. C. Meecham and A. Siegel, *Phys. Fluids* **7**:1178 (1964).